Magnetic and thermodynamic studies on the distorted kagome magnet Pr_3BWO_9

A. Elghandour,[1,2] J. Arneth,[1] A. Yadav,[3] S. Luther,[4] P. Khuntia,[3,5,*] and R. Klingeler[1,†]

[1]*Kirchhoff Institute for Physics, Heidelberg University, INF 227, D-69120 Heidelberg, Germany*

[2]*European XFEL, D-22869 Schenefeld, Germany*

[3]*Department of Physics, Indian Institute of Technology Madras, Chennai 600036, India*

[4]*Dresden High Magnetic Field Laboratory (HLD-EMFL), Helmholtz-Zentrum Dresden-Rossendorf, 01328 Dresden, Germany*

[5]*Quantum Centre of Excellence for Diamond and Emergent Materials, Indian Institute of Technology Madras, Chennai 600036, India*

(Received 30 April 2025; accepted 13 June 2025; published 10 July 2025)

We report specific heat, ac/dc magnetic susceptibility as well as static and pulsed field magnetization studies on the distorted kagome magnet Pr_3BWO_9 down to 0.4 K and up to high magnetic fields. The low-temperature thermodynamic properties are found to be governed by an electronic quasidoublet ground state, the energy splitting of which amounts to $\Delta_1 \simeq 18$ K and exhibits a quadratic field dependence with $g_{\rm eff} = 2.6$. Fitting of the specific heat data implies that the next excited state is strongly gapped at $\Delta_2 = 430$ K and threefold degenerate in zero field. Our dc and ac susceptibility studies down to 0.4 K do not detect signatures of distinct spin glass behavior. Pulsed field magnetization measurements up to 60 T confirm the Ising-like paramagnetic nature of the magnetic ground state, which is characterized by $m_J = \pm 4$ and the anisotropy energy $E_a \simeq 950$ K.

DOI: 10.1103/43bm-x8cj

I. INTRODUCTION

Frustrated quantum magnets, in which a delicate interplay among emergent degrees of freedom is active, serve as excellent candidate materials for hosting a wide array of exotic many-body phenomena that transcend conventional paradigms [1–8]. In lanthanide-based materials with strong geometric frustration, a rich variety of exotic magnetic ground states can be studied by varying between the Heisenberg and Ising limits, and between the quasiclassical and quantum limits, through appropriate choice of the rare earth ions. Due to strong intrinsic spin-orbit coupling in the $4f$ shell and often dominant dipolar magnetic interactions, rare earth-hosting systems avoid perturbations found in $3d$ transition-metal-based candidate materials and, hence, hold promise to realize novel spin liquid states. The localized nature of the $4f$ electrons typically leads to weak magnetic interaction energies, such that spin dynamics associated with geometrical frustration often emerge at low temperatures far below the first excited crystal field level, while rather moderate, i.e., accessible, magnetic fields are sufficient to cover the full energy range. Prominent examples of such material families are pyrochlores $R_2Ti_2O_7$ [9–13], filled hexagonal lattice indates $RInO_3$ [14,15], langasites $R_3Ga_5SiO_{14}$ [16–18], triangular $NdTa_7O_{19}$ [19], or the tripod kagome magnets $R_3Mg_2Sb_3O_{14}$ [20–23].

Boratotungstates R_3BWO_9 have recently entered the stage as a new family of frustrated quantum magnets [24–30]. Among them, Pr_3BWO_9 in particular exhibits no long-range magnetic order down to at least 90 mK [26,29]. The material crystallizes in a hexagonal coordinated structure with space group $P6_3$ where the paramagnetic Pr^{3+} ions form a distorted kagome lattice within the ab planes which are stacked in an AB-type fashion along the c axis [24,26,28] (see Fig. 1). The distorted kagome lattice features triangles of two different Pr-Pr bond lengths with 4.312 Å and 4.886 Å, respectively, arranged in an alternating pattern. Two recent studies have investigated the magnetic ground state as well as low-energy magnetic excitations. A recent NMR study [26] shows a persistent cooperative paramagnetic state at lowest temperatures and suggests a spin gap opening at the antiferromagnetic wave vector, the size of which is linearly increasing in external magnetic fields. These results are contrasted by inelastic neutron scattering, heat capacity, ultrasound, and muon spin relaxation measurements, which suggest a quantum disordered ground state [29]. The observed data are explained in terms of dispersive crystal field excitations partially broadened by weak structural disorder and hence suggest that Pr_3BWO_9 is not a perfect kagome magnet but realizes a complex exchange topology of twisted triangular spin tubes, moderately coupled by the frustrated planar interactions.

Here, we report detailed specific heat as well as dc and ac magnetic studies on Pr_3BWO_9 up to high magnetic fields. No evidence of long-range order nor of glassy behavior is observed in our dc and ac magnetization studies down to 400 mK. The magnetic ground state is further investigated by magnetization studies up to 60 T confirming its Ising-like paramagnetic nature. In addition to the anisotropy energy $E_a \simeq 82$ meV, we determine the energy levels of the five lowest lying states of Pr^{3+} and investigate the field dependence of the smallest excitation gap.

II. EXPERIMENTAL METHODS

A polycrystalline sample of Pr_3BWO_9 was prepared using a solid-state reaction method. The starting materials Pr_6O_{11} (Alfa Aesar, 99.999%), W_3BO_3 (Alfa Aesar, 98%), and WO_3 (Alfa Aesar, 99.998%) were taken in a stoichiometric ratio

*Contact author: pkhuntia@iitm.ac.in

†Contact author: klingeler@kip.uni-heidelberg.de

 ©2025 American Physical Society

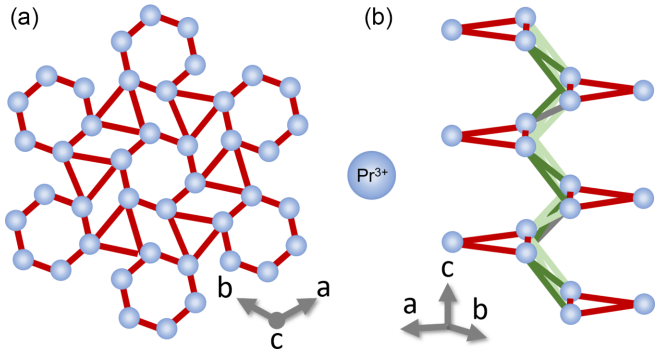

FIG. 1. Schematics of the Pr^{3+} sites (blue spheres) in Pr_3BWO_9. (a) In-plane (*ab* plane) arrangement and (b) stacking along the *c* axis. Lines indicate short in-plane (red) and interplanar (green) Pr-Pr distances.

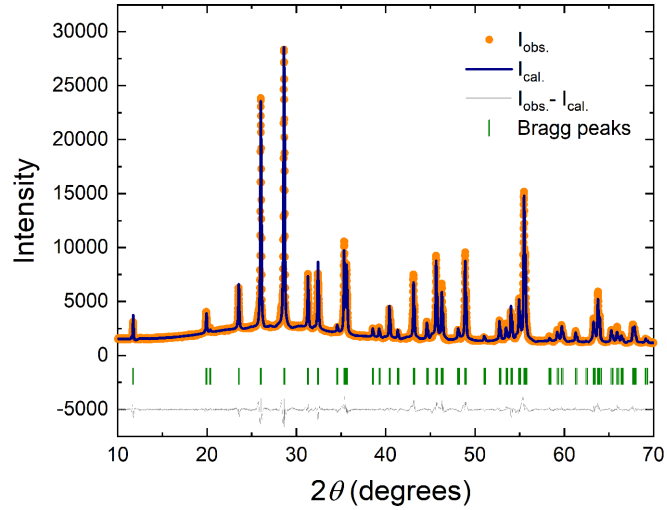

FIG. 2. Rietveld refinement of XRD data of Pr_3BWO_9 taken at room temperature. The orange circles, blue solid lines, olive vertical bars, and gray solid lines are the observed data, calculated data, Bragg peaks, and difference of observed and calculated data of Pr_3BWO_9, respectively.

[29,31]. The reagent W_3BO_3 is highly volatile; therefore, we added 5% excess to maintain proper stoichiometry in the sample. Pr_6O_{11} was preheated at 900 °C for 12 h to remove moisture and carbonates prior to use. All the reagents were thoroughly mixed to ensure better homogeneity. An alumina crucible was used to anneal the pellets in the temperature range of 700–900 °C, with several intermediate grindings. X-ray diffraction (XRD) was recorded on the polycrystalline sample of Pr_3BWO_9 at room temperature using a bench-top PANalytical diffractometer with Cu $K\alpha$ radiation ($\lambda = 1.541$ Å). The XRD data were recorded from 10° to 70° with a step size of 0.01 for 1 h. The Rietveld refinement of the XRD pattern at room temperature aims to confirm the phase purity and crystallographic parameters employing FULLPROF software [32]. The site occupancies were kept fixed during the refinement as this is a known structure and there is no site disorder observed in this family of kagome compounds. The Rietveld refinement reveals that the samples used in this study are of high quality and the refinement parameters are consistent with those reported earlier. Figure 2 depicts the corresponding refinement pattern at room temperature and the associated refinement parameters are documented in Table I.

Magnetic measurements were performed on pressed pellets of $m = 6.6(2)$ mg in a MPMS3 magnetometer (Quantum Design) in the temperature regime of 1.8 to 350 K. For measurements down to 400 mK, the MPMS3 was equipped with the iQuantum ^{3}He setup. The static magnetic susceptibility $\chi = M/B$ has been obtained by varying the temperature using field cooled (FC) and zero field cooled (ZFC) protocols where the sample was cooled in either the external measurement field or the field was applied after cooling to the lowest temperature, respectively. Isothermal magnetization $M(B)$ has been measured in fields up to $B = 7$ T. ac magnetization measurements were conducted in the temperature range from 1.8 to 60 K, with 5–7 Oe ac excitation fields, up to 5 T dc magnetic fields, and at frequencies ranging from 10 to 800 Hz. These measurements were conducted using the ac option of the MPMS3 on a sample with a mass of $m = 2.3(1)$ mg.

Pulsed-field magnetization was measured up to 60 T at Helmholtz Zentrum Dresden-Rossendorf (HLD) by an induction method using a coaxial compensated pick-up coil system [33]. The pulse raising time was 7 ms. Each measurement of the sample was followed by recording the background without a sample under identical conditions, to compensate for background contributions. The pulsed-field magnetization data were calibrated using static magnetic field magnetization data obtained by means of the MPMS3. The field dependence of magnetization obtained by the two methods is in good agreement, which confirms the accuracy of our experiments.

To measure the specific heat capacity of the samples, a relaxation method was employed using the heat capacity option of the Physical Property Measurement System (PPMS-14) by Quantum Design. The measurements were carried out in the temperature regime from 1.8 to 200 K on a sample with a mass of 6.6(2) mg under applied magnetic fields up to 14 T.

TABLE I. Crystallographic parameters determined from the Rietveld refinement of XRD data of Pr_3BWO_9 recorded at room temperature (see Fig. 2). [Space group $P6_3$, lattice parameters $a = b = 8.7299(1)$ Å and $c = 5.5230(1)$ Å, occupation factor was fixed to one for all sites, $\chi^2 = 7.7$, $R_{wp} = 5.84\%$, $R_p = 4\%$, and $R_{exp} = 2.1\%$.]

Atom	Wyckoff pos.	x	y	z	B_{iso}
Pr	6*c*	0.0838(1)	0.7246(1)	0.3615(9)	0.269(4)
B	2*a*	0.0000	0.0000	0.0000	0.491(9)
W	2*b*	0.3333	0.6666	0.8884(9)	0.293(6)
O1	6*c*	0.053(2)	0.885(2)	1.010(3)	0.652(7)
O2	6*c*	0.105(2)	0.485(1)	0.153(2)	0.486(5)
O3	6*c*	0.191(2)	0.435(2)	0.672(2)	0.978(8)

III. RESULTS AND DISCUSSION

A. Dc, ac, and pulsed field magnetization

The static magnetic susceptibility of Pr_3BWO_9 at $B = 1$ T, shown in Fig. 3, decreases upon heating and does not exhibit

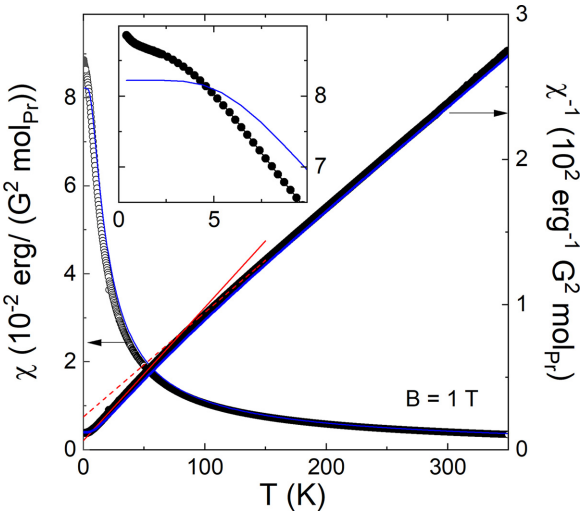

FIG. 3. Temperature dependence of the static magnetic susceptibility $\chi = M/B$ and its inverse χ^{-1} (with reduced number of data points for visibility) measured at $B = 1$ T. The dashed (solid) red line represents high (low) temperature Curie-Weiss fits to the data (see the text). The blue line depicts the simulation of a noninteracting single ion model for Pr^{3+} using the crystal field parameters obtained in Ref. [29]. The inset shows the enlargement of the low-temperature regime.

any pronounced anomalies in the whole temperature regime $0.4\ \text{K} \leqslant T \leqslant 350\ \text{K}$ under study. In particular, the data do not show any signature of long-range magnetic order down to 400 mK, which is in agreement with recent specific heat, inelastic neutron, and μSR data [26,29]. In the literature, absence of long-range magnetic order down to at least 90 mK [26] is reported. The low-temperature $\chi(T)$ indicates saturation below $\simeq$5 K superimposed by a small upturn starting from $\sim$0.7 K. Based on the observation of a weak FC/ZFC bifurcation which amounts to less than 0.2% of the magnetization signal in the same temperature regime [Fig. 4(a)], the

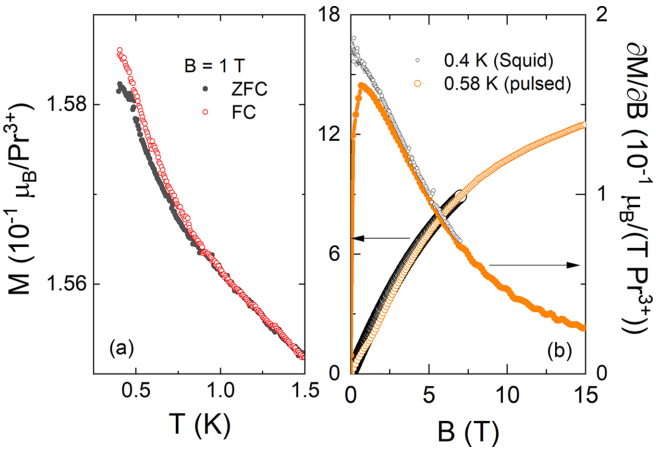

FIG. 4. (a) Temperature dependence of the static susceptibility, at $T < 1.5$ K, and (b) field dependence of the magnetization and of the differential magnetic susceptibility $\partial M/\partial B$, at low temperature. Black open (orange filled) data points refer to static (pulsed) field measurements.

latter is likely not associated with quasifree moments from putative defects but might rather be related to a spin freezing phenomenon typically observed in spin glass materials [13,34–36]. This scenario is in qualitative agreement with the observation of a peak at $B = 0.7$ T and $M/M_{\text{sat}} \sim 1/5$ in the pulsed field $\partial M/\partial B$ data at $T \simeq 0.5$ K, which is absent in the static field measurements [Fig. 4(b)]. Our results, thus, indicate that a tiny fraction of Pr^{3+} moments start to freeze below $\sim$0.7 K, while the bulk of the spins maintains a dynamic state.

At high temperatures, $\chi(T)$ exhibits a Curie-Weiss-like behavior. Fitting the data between $150\ \text{K} \leqslant T \leqslant 350$ K by means of the Curie-Weiss model yields an effective magnetic moment of $p_{\text{eff}} = 3.33(3)\mu_{\text{B}}$ and the Weiss temperature $\Theta_{\text{high}} = -31(2)$ K in agreement with previous reports [24]. While the negative sign of Θ_{high} indicates dominant antiferromagnetic interactions, p_{eff} is smaller than the theoretical free ion value of $3.58\mu_{\text{B}}$ for Pr^{3+}. As will be shown when discussing specific heat data, we attribute this deviation from the free ion value to the presence of crystal field levels of Pr^{3+} which are not (fully) thermally populated at the highest measurement temperature of 350 K. We in particular note that employing the noninteracting single-ion crystal-field model from Ref. [29] yields a good description of our magnetic susceptibility data (cf. Fig. 3) which implies very weak or nearly vanishing magnetic interaction. Note that an estimate of bare magnetic dipolar interaction energy yields $E_{\text{dip}} < 0.2$ K. We conclude that the data only seemingly resemble a Curie-Weiss-like behavior at intermediate temperatures but actually are dominated by the thermal population of excited crystal field levels. Upon cooling, a second quasilinear regime is observed in χ^{-1} below $\sim$40 K (see Fig. 3). Fitting the data in the temperature regime $10\ \text{K} \leqslant T \leqslant 25$ K results in $p_{\text{eff}} = 2.95(1)\ \mu_{\text{B}}$ and $\Theta_{\text{low}} = -6.8(2)$ K, which are consistent with those reported in Refs. [24,26,29]. This behavior reflects the subsequent depopulation of Pr^{3+} crystal field levels so that neither Θ_{high} nor Θ_{low} can be taken as a reliable measure of the strength of magnetic interaction and, in contrast to previous reports, we suggest that it should not be used to estimate the frustration parameter.

The ac magnetic susceptibility of Pr_3BWO_9 shows neither a dissipative signal in the imaginary part χ'' (data not shown) nor any frequency dependence in the real part within the studied temperature and frequency range, i.e., at $T \geqslant 1.8$ K and $10\ \text{Hz} \leqslant f \leqslant 600$ Hz. Consistent with the static susceptibility shown in Fig. 3, the real part of ac susceptibility χ' increases monotonically upon cooling. The frequency independence implies that at $T \geqslant 1.8$ K, which is well above the temperature regime where the tiny bifurcation is observed in $\chi_{\text{dc}}(T)$ [cf. Fig. 4(a)], Pr_3BWO_9 either displays no glassy behavior or the characteristic spin-fluctuation rate in Pr_3BWO_9 is beyond the kilohertz frequency regime. The latter scenario is suggested by NMR studies (MHz frequencies) revealing the existence of short-ranged collective spin excitations [26]. The application of external dc magnetic fields barely affects the behavior of $\chi'(T)$ as seen in Fig. 5 and, in particular, does not induce clear anomalies. Note that this is in stark contrast to the findings in Nd_3BWO_9 [30], thereby demonstrating strong differences in the spin relaxation rates of the two systems. One may speculate that spin relaxation rates in Pr_3BWO_9 are much higher than those in Nd_3BWO_9 where already moderate

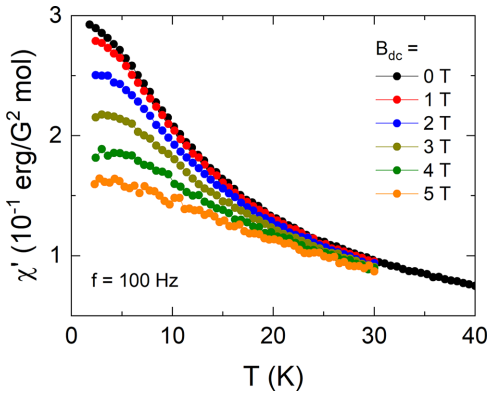

FIG. 5. Temperature dependence of the real part of the ac magnetic susceptibility χ' measured at $f = 100$ Hz and $B_{ac} = 0.5$ mT, at different static magnetic fields. Changing the frequencies in the range of 10 Hz $\leqslant f \leqslant$ 800 Hz yields no changes of the signal (data not shown).

magnetic fields of a few tesla induce slow spin relaxation at tens of kelvin while spin freezing appears at 0.6 K.

The magnetization at low temperature increases quasilinearly up to $\simeq$2 T and shows right bending at higher magnetic field without any clear additional features (Figs. 4 and 6). At the maximum applied magnetic field of 58 T and $T = 3$ K, M amounts to $1.60(2)\mu_B/Pr^{3+}$. Extrapolating the linear-in-field regime which is observed at $B > 30$ T to zero magnetic field yields $1.2\mu_B/Pr^{3+}$. In a pure paramagnet, this value reflects the saturation magnetization of the powder averaged ground state singlet. Considering an almost uniaxial crystal field and $g_J = 4/5$ of the free ion, and powder averaging, this suggests an Ising ground state with $|m_J| = 4$. Our data also allow us to roughly estimate the anisotropy field by linearly extrapolating the pulsed field magnetization up to the full

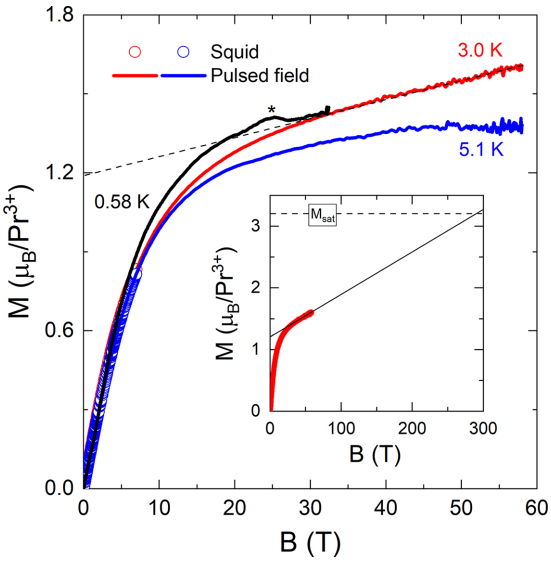

FIG. 6. Magnetic field dependence of the static and the pulsed field magnetization of Pr_3BWO_9 measured at different temperatures in up-sweeps of magnetic fields up to 7 T and 58 T, respectively. The asterisk marks an experimental artifact. Inset: $M(T = 3\text{ K}, B)$ extrapolated up to the saturation value $M_{sat} = 3.2\mu_B/Pr^{3+}$.

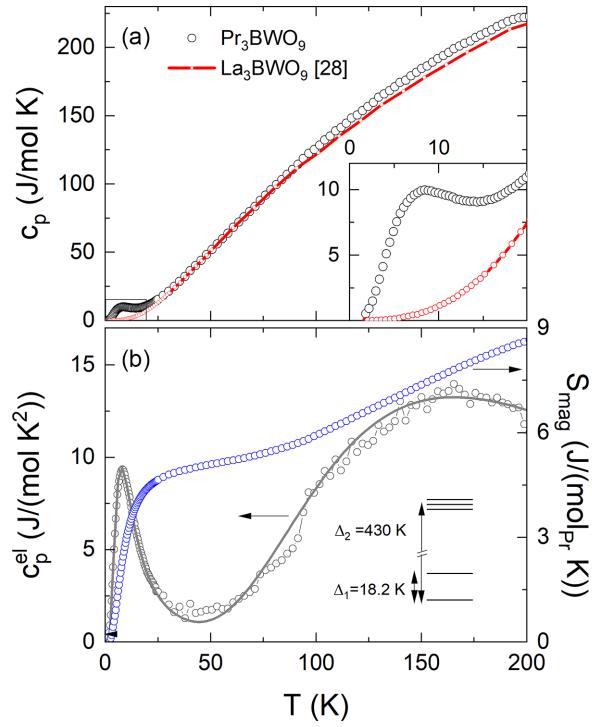

FIG. 7. Temperature dependence of (a) the specific heat of Pr_3BWO_9 and La_3BWO_9 measured at $B = 0$ T; the latter data are taken from Ref. [28]. Inset: enlargement of the low-temperature regime. (b) Nonphononic specific heat c_p^{el} of Pr_3BWO_9 as obtained by the subtraction of c_p La_3BWO_9 from the one of Pr_3BWO_9, and calculated magnetic entropy $S_{mag} = \int[c_p^{el}(T)/T]dT$. The line is a fit according to an extended three-level Schottky model [see Eq. (3)] with $\Delta_1 = 18.2$ K, $\Delta_2 = 430$ K, and level degeneracies $g_0 = 1$, $g_1 = 1$, and $g_2 = 3$ (see the text).

saturation magnetization of $3.2\mu_B/Pr^{3+}$ associated with the complete alignment of Pr^{3+} moments of the powder sample along the magnetic field direction: following the dashed line in Fig. 6 suggests a saturation field of $B_{sat} \simeq 300(25)$ T (inset of Fig. 6).[1] We hence conclude the anisotropy energy $E_a/k_B = g_J\mu_B m_J B \simeq 950$ K ($E_a \simeq 82$ meV). In summary, our pulsed field magnetization data suggest a strong uniaxial crystal field and an Ising ground state in Pr_3BWO_9 characterized by a (mainly) $m_J = -4$ ground state singlet, in agreement to Ref. [29]. This finding implies the dominance of anisotropy energy over magnetic exchange interactions which is consistent with the observed absence of a 1/3 magnetization plateau (in the pulsed field data) or a 1/9 plateau (which would also show up in the MPMS3-static field data), which are typically observed in Heisenberg-like kagome antiferromagnets (see, e.g., Refs. [37–41]).

B. Heat capacity

The electronic contribution to the specific heat capacity of Pr_3BWO_9 is estimated by subtracting the phononic

[1]Deviations from linear field dependence cannot be excluded so that we do not provide error bars of our following estimate of anisotropy energy.

contribution of the isostructural nonmagnetic La_3BWO_9 as reported for $T < 200$ K in Ref. [28]. In order to account for the different molar masses, the scaling factor of 0.97 (see Ref. [42]) has been applied. The resulting c_p^{el} is presented in Fig. 7(b) and features a peak centered at around 5.7 K, which is well separated from an additional, much broader hump at higher temperatures. The electronic specific heat is attributed to electronic or, specifically, magnetic degrees of freedom. The entropy changes in the temperature regime 1.8–40 K, i.e., $\Delta S_{mag} = \int_{1.8\ K}^{40\ K} [c_p^{el}(T)/T] dT$ associated with the low-temperature peak amount to 4.9 J/(mol$_{Pr}$ K). Adding the entropy changes of 0.11 J/(mol$_{Pr}$ K) from the heat capacity data at 0.09 K $\leqslant T \leqslant$ 1.8 K reported in Ref. [26], S_{mag} amounts to only 30% of the full expected magnetic entropy of R ln(8) = 18.3 J/(mol$_{Pr}$ K) for $J = 4$, but it represents 86% of the expected value [R ln 2 = 5.76 J/(mol$_{Pr}$ K)] of a two-level system with $J_{eff} = 1/2$, where R is the universal gas constant. We note that in the isomorphic Nd_3BWO_9 the magnetic entropy changes are, too, well described by a two-level system [28,30] but in the Nd-based sister compound the magnetic entropy is released below $T = 3$ K, i.e., at one-tenth of the saturation temperature of the lowest energy gap found in Pr_3BWO_9.

The broad anomaly in the electronic specific heat centered around 8 K shown in Fig. 7 resembles a Schottky-like behavior and can be attributed to electronic excitations within the split $J = 4$ ground state manifold of the Pr^{3+} ions [26,29]. The Schottky nature is clearly corroborated by the observed magnetic field dependence which shows a gradual shift of the peak position to higher temperatures, peak broadening, and peak height suppression upon application of external magnetic fields [cf. Fig. 8(a)]. The low-temperature peak is associated with the energy gap between the lowest crystal field-split energy levels and, hence, can be used to investigate, e.g., the gap size and magnetic field dependence and the degeneracies of the associated energy levels. For the non-Kramer's ion Pr^{3+} with $J = 4$, the crystal field effects in Pr_3BWO_9 result in nine singlet states, some of which may have accidental or near degeneracies [26,29,43]. To quantify the energy gap separation between the ground state and the first excited level, the Schottky model for the specific heat capacity of a gapped two-level system is fitted to the data [42]:

$$c_p^{\Delta_1} = n \cdot R \left(\frac{\Delta_1}{T}\right)^2 \frac{g_0}{g_1} \frac{e^{\frac{\Delta_1}{T}}}{\left[1 + \left(\frac{g_0}{g_1}\right) e^{\frac{\Delta_1}{T}}\right]^2}. \quad (1)$$

Here, n is the concentration of magnetic sites, R is the universal gas constant, Δ_1 is the associated energy gap, and (g_0/g_1) is the degeneracy ratio of the two energy levels. Using n and Δ_1 as free fit parameters while fixing $g_0/g_1 = 1$ yields a good description of the experimental data c_p^{el} as represented by the solid lines in Fig. 8(a). The resulting fit parameters are listed in Table II. We note that the best fits are achieved with g_0/g_1 kept constant, which implies that the magnetic field effect on the levels' degeneracies is negligible. Further, the fits yield essentially field independent $n \simeq 2.6$, which indicates that only 85% of the Pr^{3+} ions contribute to the Schottky specific heat. This agrees well with the observed entropy changes of $\sim 0.85 \times R$ ln 2.

The magnetic field dependence of the obtained Δ is plotted in Fig. 8(b). It is well described by the expected quadratic

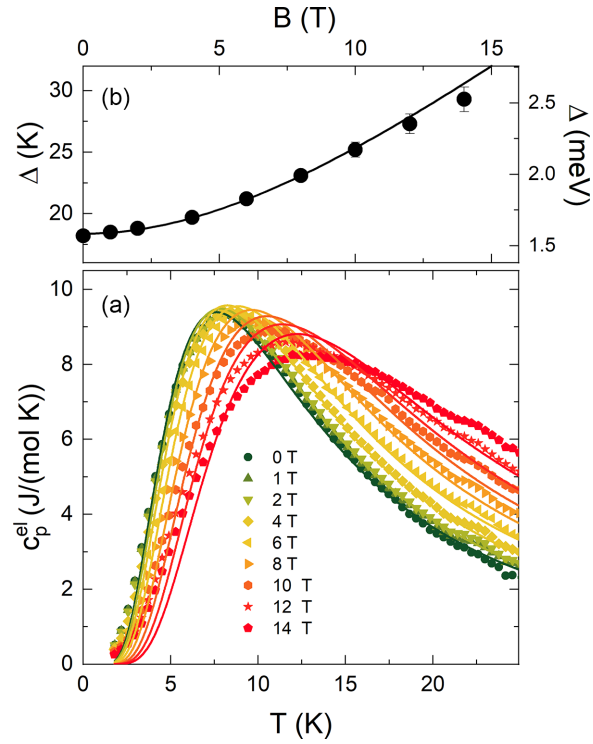

FIG. 8. (a) Temperature dependence of the electronic specific heat c_p^{el} of Pr_3BWO_9 for different applied magnetic fields. The solid lines represent the fits to the two-level Schottky function according to Eq. (1). (b) Magnetic field dependence of the energy gap Δ_1 obtained from the fitting c_p with the Schottky model. The line illustrates the cubic field dependence of Δ.

behavior

$$\Delta_1(B) = \sqrt{[\Delta_1(0)]^2 + (g\mu_B B/k_B)^2}, \quad (2)$$

with $\Delta_1(0) = \Delta_1(B = 0\ T)$ and the effective g factor, g. The best fit yields $\Delta_1(0) = 18.4$ K (i.e., 1.6 meV). This value agrees very well with the excitation gap of 1.62(1) meV found in inelastic neutron scattering [29] but is considerably larger than the excitation gap of 8.0 K (14.1 K) found in NMR for the $B||c$ ($B \perp c$) axis [26]. The field dependence is best described by $g \simeq 2.6$, which is in very good agreement with

TABLE II. Parameters describing the electronic specific heat c_p^{el} obtained by fitting the data to a two-level Schottky [Eq. (1)] model at different applied magnetic fields (see Fig. 8). Δ_1 is the splitting gap and n is the concentration of Schottky centers.

B (T)	n	Δ_1 (K)
0	2.57(1)	18.2(1)
1	2.58(1)	18.5(1)
2	2.57(1)	18.9(1)
4	2.62(2)	19.8(2)
6	2.61(2)	21.2(2)
8	2.58(1)	23.1(2)
10	2.54(2)	25.2(3)
12	2.48(2)	27.3(4)
14	2.41(1)	29.5(6)

the powder average of the Ising-like low-energy m_J states as described by the crystal field parameters in Ref. [29]. The observed quadratic dependence $\Delta_1(B)$ qualitatively resembles the findings of Ref. [29], while Ref. [26] reports a linear field dependence of Δ. Note that the pulsed field magnetization data in Fig. 6 do not indicate field-induced level crossing, e.g., closing of the gap Δ_1. Such a closing of the gap would be observed in the high-field measurements if, e.g., the first excited singlet was characterized by larger (i.e., more negative) effective m_J as compared to the ground state. This observation is in agreement with the Ising-like scenario.

The second hump in c_p^{el} appearing around 160 K indicates the thermal population of one or more energetically higher-lying crystal field levels of Pr^{3+}. We hence extend the Schottky model Eq. (1), which is used to describe the entropy changes associated with the thermal population of the crystal field levels to a three-level model [44]:

$$c_p^{\Delta_1/\Delta_2} = nR \times \frac{g_1 g_0 \Delta_1^2 g_1 e^{-\Delta_1/T} + g_0 g_2 \Delta_2^2 g_1 e^{-\Delta_2/T} + g_1 g_2 e^{-(\Delta_1+\Delta_2)/T}[\Delta_1(\Delta_1-\Delta_2)+\Delta_2(\Delta_2-\Delta_1)]}{T^2[g_0 + g_1 e^{-\Delta_1/T} + g_2 e^{-\Delta_2/T}]^2}. \quad (3)$$

Here, the energies of the three lowest states are 0, Δ_1, and Δ_2, while g_i ($i = 0, 1, 2$) is the degeneracy of the respective level. Fitting the experimental data by means of Eq. (3) yields an excellent description of the data. Using $n = 2.6$ obtained from the low-temperature Schottky peak, c_p^{el} is well described by $\Delta_1 = 18.2$ K and $\Delta_2 = 430$ K [see the gray line and the sketch in Fig. 7(b)]. While the degeneracies of the ground state and the first excited state are $g_0 = 1$ and $g_1 = 1$, the second excited state exhibits $g_2 = 3$. These results are in reasonable agreement with crystal field splittings suggested by a point-charge model in Ref. [29], which predicts a ground state quasidoublet while the next excited states are well isolated singlets at energies of $\Delta_2 = 429$ K (37.0 meV), $\Delta_3 = 494$ K (42.6 meV), and $\Delta_4 = 673$ K (58.0 meV). However, as clearly seen in the experimental data, the predicted gap values neither are consistent with our specific heat nor do we find signatures for well separated singlets at the predicted energies Δ_2, Δ_3, and Δ_4. In contrast, the experimental data imply three quasidegenerated levels. Quantitatively, our data support a slightly smaller value of Δ_2 than predicted by the point-charge model and clearly disagree with the prediction for Δ_4.

C. Summary

In summary, we report detailed dc and ac magnetization studies of the frustrated kagome system Pr_3WBO_9 in a wide magnetic field and temperature regime, i.e., up to 60 T in pulsed magnetic fields and up to 7 T in static fields and down to 0.4 K. This is supported by specific heat studies up to 14 T. Our data confirm a highly frustrated Ising-like system the low-temperature properties of which are governed by two moderately split singlets ($\Delta_1 \simeq 18$ K) forming a quasidoublet well separated from all other crystal field levels. The next excited states are identified at $\Delta_2 \simeq 430$ K. The low-energy gap Δ_1 increases quadratically in external magnetic fields and the field dependence is governed by the effective g factor 2.6. No distinct glassy behavior is observed in our dc and ac magnetization studies down to 400 mK. The magnetic ground state is further investigated by magnetization studies up to 60 T confirming the Ising-like paramagnetic nature of the magnetic ground state, which is mainly characterized by $m_J = -4$ with anisotropy energy $E_a/k_B \simeq 950$ K. The magnetic susceptibility is well described by an isolated single-ion model. Our results hence add Pr_3BWO_9 to the growing family of Ising-like yet disordered complex lanthanide-based magnets. Additional studies of magnetic excitations and magnetic exchange interactions on high-quality single crystals will be needed to further elucidate the quantum Ising ground state and associated excitations in this class of frustrated quantum magnets.

ACKNOWLEDGMENTS

Support by Deutsche Forschungsgemeinschaft (DFG) under Germany's Excellence Strategy EXC2181/1-390900948 (The Heidelberg STRUCTURES Excellence Cluster) is gratefully acknowledged. A.E. acknowledges funding through the DAAD GSSP program. We acknowledge the support of the HLD at HZDR, a member of the European Magnetic Field Laboratory. J.A. acknowledges support by the IMPRS-QD Heidelberg. P.K. acknowledges the funding by the Science and Engineering Research Board and Department of Science and Technology, India through Research Grants.

DATA AVAILABILITY

The data that support the findings of this article are not publicly available. The data are available from the authors upon reasonable request.

[1] L. Balents, Spin liquids in frustrated magnets, Nature (London) **464**, 199 (2010).

[2] C. Broholm, R. J. Cava, S. A. Kivelson, D. G. Nocera, M. R. Norman, and T. Senthil, Quantum spin liquids, Science **367**, eaay0668 (2020).

[3] Y. Zhou, K. Kanoda, and T.-K. Ng, Quantum spin liquid states, Rev. Mod. Phys. **89**, 025003 (2017).

[4] S. Nishimoto, S.-L. Drechsler, R. O. Kuzian, J. van den Brink, J. Richter, W. E. A. Lorenz, Y. Skourski, R. Klingeler, and B. Büchner, Saturation field of frustrated chain cuprates: Broad regions of predominant interchain coupling, Phys. Rev. Lett. **107**, 097201 (2011).

[5] W. E. A. Lorenz, R. O. Kuzian, S.-L. Drechsler, W.-D. Stein, N. Wizent, G. Behr, J. Málek, U. Nitzsche, H. Rosner, A. Hiess,

W. Schmidt, R. Klingeler, M. Loewenhaupt, and B. Büchner, Highly dispersive spin excitations in the chain cuprate Li_2CuO_2, Europhys. Lett. **88**, 37002 (2009).

[6] L. Savary and L. Balents, Quantum spin liquids: A review, Rep. Prog. Phys. **80**, 016502 (2017).

[7] J. Khatua, B. Sana, A. Zorko, M. Gomilšek, K. Sethupathi, M. R. Rao, M. Baenitz, B. Schmidt, and P. Khuntia, Experimental signatures of quantum and topological states in frustrated magnetism, Phys. Rep. **1041**, 1 (2023).

[8] N. Yuan, E. Walendy, N. Maraytta, W. Hergett, L. Bischof, M. Merz, and R. Klingeler, Anisotropic magnetic phase diagrams, tricriticality, and spin reorientation in high-pressure grown $SmCrO_3$ single crystals, Phys. Rev. B **111**, 174437 (2025).

[9] A. P. Ramirez, A. Hayashi, R. J. Cava, R. Siddharthan, and B. Shastry, Zero-point entropy in 'spin ice', Nature (London) **399**, 333 (1999).

[10] S. T. Bramwell and M. J. Gingras, Spin ice state in frustrated magnetic pyrochlore materials, Science **294**, 1495 (2001).

[11] L. Savary, K. A. Ross, B. D. Gaulin, J. P. C. Ruff, and L. Balents, Order by quantum disorder in $Er_2Ti_2O_7$, Phys. Rev. Lett. **109**, 167201 (2012).

[12] J. A. M. Paddison, G. Ehlers, A. B. Cairns, J. S. Gardner, O. A. Petrenko, N. P. Butch, D. D. Khalyavin, P. Manuel, H. E. Fischer, H. Zhou, A. L. Goodwin, and J. R. Stewart, Suppressed-moment 2-k order in the canonical frustrated antiferromagnet $Gd_2Ti_2O_7$, npj Quantum Mater. **6**, 99 (2021).

[13] A. Elghandour, Sheetal, C. S. Yadav, and R. Klingeler, Slow spin relaxation and low-temperature spin freezing in the disordered fluorite $Ho_2Zr_2O_7$, Phys. Rev. B **110**, 064408 (2024).

[14] L. Clark, G. Sala, D. D. Maharaj, M. B. Stone, K. S. Knight, M. T. Telling, X. Wang, X. Xu, J. Kim, Y. Li *et al.*, Two-dimensional spin liquid behaviour in the triangular-honeycomb antiferromagnet $TbInO_3$, Nat. Phys. **15**, 262 (2019).

[15] N. Yuan, A. Elghandour, W. Hergett, R. Ohlendorf, L. Gries, and R. Klingeler, 1/3 plateau and 3/5 discontinuity in the magnetization and the magnetic phase diagram of hexagonal $GdInO_3$, Phys. Rev. B **108**, 224403 (2023).

[16] H. D. Zhou, B. W. Vogt, J. A. Janik, Y.-J. Jo, L. Balicas, Y. Qiu, J. R. D. Copley, J. S. Gardner, and C. R. Wiebe, Partial field-induced magnetic order in the spin-liquid kagomé $Nd_3Ga_5SiO_{14}$, Phys. Rev. Lett. **99**, 236401 (2007).

[17] V. Simonet, R. Ballou, J. Robert, B. Canals, F. Hippert, P. Bordet, P. Lejay, P. Fouquet, J. Ollivier, and D. Braithwaite, Hidden magnetic frustration by quantum relaxation in anisotropic Nd langasite, Phys. Rev. Lett. **100**, 237204 (2008).

[18] L. Weymann, L. Bergen, T. Kain, A. Pimenov, A. Shuvaev, E. Constable, D. Szaller, B. V. Mill, A. M. Kuzmenko, V. Y. Ivanov, N. V. Kostyuchenko, A. I. Popov, A. K. Zvezdin, A. Pimenov, A. A. Mukhin, and M. Mostovoy, Unusual magnetoelectric effect in paramagnetic rare-earth langasite, npj Quantum Mater. **5**, 61 (2020).

[19] T. Arh, B. Sana, M. Pregelj, P. Khuntia, Z. Jagličić, M. D. Le, P. K. Biswas, P. Manuel, L. Mangin-Thro, A. Ozarowski, and A. Zorko, The Ising triangular-lattice antiferromagnet neodymium heptatantalate as a quantum spin liquid candidate, Nat. Mater. **21**, 416 (2021).

[20] Z. L. Dun, J. Trinh, K. Li, M. Lee, K. W. Chen, R. Baumbach, Y. F. Hu, Y. X. Wang, E. S. Choi, B. S. Shastry, A. P. Ramirez, and H. D. Zhou, Magnetic ground states of the rare-earth tripod kagome lattice $Mg_2Re_3Sb_3O_{14}$ (RE = Gd, Dy, Er), Phys. Rev. Lett. **116**, 157201 (2016).

[21] J. A. M. Paddison, H. S. Ong, J. O. Hamp, P. Mukherjee, X. Bai, M. G. Tucker, N. P. Butch, C. Castelnovo, M. Mourigal, and S. E. Dutton, Emergent order in the kagome Ising magnet $Dy_3Mg_2Sb_3O_{14}$, Nat. Commun. **7**, 13842 (2016).

[22] J. Khatua, M. Pregelj, A. Elghandour, Z. Jagličic, R. Klingeler, A. Zorko, and P. Khuntia, Magnetic properties of the triangular-lattice antiferromagnets $Ba_3Rb_9O_{18}$ (R = Yb, Er), Phys. Rev. B **106**, 104408 (2022).

[23] C. Wellm, J. Zeisner, A. Alfonsov, M.-I. Sturza, G. Bastien, S. Gaß, S. Wurmehl, A. U. B. Wolter, B. Büchner, and V. Kataev, Magnetic interactions in the tripod kagome antiferromagnet $Mg_2Gd_3Sb_3O_{14}$ probed by static magnetometry and high-field ESR spectroscopy, Phys. Rev. B **102**, 214414 (2020).

[24] M. Ashtar, J. Guo, Z. Wan, Y. Wang, G. Gong, Y. Liu, Y. Su, and Z. Tian, A new family of disorder-free rare-earth-based kagome lattice magnets: Structure and magnetic characterizations of Re_3BwO_9 (Re = Pr, Nd, Gd–Ho) boratotungstates, Inorg. Chem. **59**, 5368 (2020).

[25] Z. Yang, H. Zhang, M. Bai, W. Li, S. Huang, S. Ruan, and Y.-J. Zeng, Large magnetocaloric effect in gadolinium borotungstate Gd_3BwO_9, J. Mater. Chem. C **8**, 11866 (2020).

[26] K. Y. Zeng, F. Y. Song, Z. M. Tian, Q. Chen, S. Wang, B. Liu, S. Li, L. S. Ling, W. Tong, L. Ma, and L. Pi, Local evidence for collective spin excitations in the distorted kagome antiferromagnet Pr_3BwO_9, Phys. Rev. B **104**, 155150 (2021).

[27] K.-Y. Zeng, F.-Y. Song, L.-S. Ling, W. Tong, S.-L. Li, Z.-M. Tian, L. Ma, and L. Pi, Incommensurate magnetic order in Sm_3BwO_9 with distorted kagome lattice, Chin. Phys. Lett. **39**, 107501 (2022).

[28] D. Flavián, J. Nagl, S. Hayashida, M. Yan, O. Zaharko, T. Fennell, D. Khalyavin, Z. Yan, S. Gvasaliya, and A. Zheludev, Magnetic phase diagram of the breathing-kagome antiferromagnet Nd_3BwO_9, Phys. Rev. B **107**, 174406 (2023).

[29] J. Nagl, D. Flavián, S. Hayashida, K. Y. Povarov, M. Yan, N. Murai, S. Ohira-Kawamura, G. Simutis, T. J. Hicken, H. Luetkens, C. Baines, A. Hauspurg, B. V. Schwarze, F. Husstedt, V. Pomjakushin, T. Fennell, Z. Yan, S. Gvasaliya, and A. Zheludev, Excitation spectrum and spin hamiltonian of the frustrated quantum Ising magnet Pr_3BwO_9, Phys. Rev. Res. **6**, 023267 (2024).

[30] A. Yadav, A. Elghandour, T. Arh, D. T. Adroja, M. D. Le, G. B. G. Stenning, M. Aouane, S. Luther, F. Hotz, T. J. Hicken, H. Luetkens, A. Zorko, R. Klingeler, and P. Khuntia, Magnetism in the $J_{\text{eff}} = \frac{1}{2}$ kagome antiferromagnet Nd_3BwO_9: Thermodynamics, nuclear magnetic resonance, muon spin resonance, and inelastic neutron scattering studies, Phys. Rev. B **111**, 094408 (2025).

[31] V. A. Krut'ko, A. A. Belik, and G. V. Lysanova, Structures of nonlinear hexagonal boratotungstates Ln_3BwO_9 (Ln = La, Pr, Nd, Sm, Gd, Tb, Dy), Russian J. Inorg. Chem. **51**, 884 (2006).

[32] J. Rodríguez-Carvajal, Recent advances in magnetic structure determination by neutron powder diffraction, Phys. B: Condens. Matter **192**, 55 (1993).

[33] Y. Skourski, M. D. Kuzmin, K. P. Skokov, A. V. Andreev, and J. Wosnitza, High-field magnetization of Ho_2Fe_{17}, Phys. Rev. B **83**, 214420 (2011).

[34] S. Nagata, P. H. Keesom, and H. R. Harrison, Low-Dc-field susceptibility of Cu Mn spin glass, Phys. Rev. B **19**, 1633 (1979).

[35] O. Petrenko, M. R. Lees, and G. Balakrishnan, Titanium pyrochlore magnets: How much can be learned from magnetization measurements? J. Phys.: Condens. Matter **23**, 164218 (2011).

[36] C. Krey, S. Legl, S. R. Dunsiger, M. Meven, J. S. Gardner, J. M. Roper, and C. Pfleiderer, First order metamagnetic transition in $Ho_2Ti_2O_7$ observed by vibrating coil magnetometry at milli-Kelvin temperatures, Phys. Rev. Lett. **108**, 257204 (2012).

[37] M. E. Zhitomirsky, Field-induced transitions in a Kagome antiferromagnet, Phys. Rev. Lett. **88**, 057204 (2002).

[38] S. Nishimoto, N. Shibata, and C. Hotta, Controlling frustrated liquids and solids with an applied field in a kagome Heisenberg antiferromagnet, Nat. Commun. **4**, 2287 (2013).

[39] J. Schnack, J. Schulenburg, and J. Richter, Magnetism of the $n = 42$ kagome lattice antiferromagnet, Phys. Rev. B **98**, 094423 (2018).

[40] R. Okuma, D. Nakamura, T. Okubo, A. Miyake, A. Matsuo, K. Kindo, M. Tokunaga, N. Kawashima, S. Takeyama, and Z. Hiroi, A series of magnon crystals appearing under ultrahigh magnetic fields in a kagomé antiferromagnet, Nat. Commun. **10**, 1229 (2019).

[41] S. Jeon, D. Wulferding, Y. Choi, S. Lee, K. Nam, K. H. Kim, M. Lee, T.-H. Jang, J.-H. Park, S. Lee, S. Choi, C. Lee, H. Nojiri, and K.-Y. Choi, One-ninth magnetization plateau stabilized by spin entanglement in a kagome antiferromagnet, Nat. Phys. **20**, 435 (2024).

[42] A. Tari, *The Specific Heat of Matter at Low Temperatures* (World Scientific, Singapore, 2003).

[43] A. Scheie, M. Sanders, J. Krizan, A. D. Christianson, V. O. Garlea, R. J. Cava, and C. Broholm, Crystal field levels and magnetic anisotropy in the kagome compounds $Nd_3Sb_3Mg_2O_{14}$, $Nd_3Sb_3Zn_2O_{14}$, and $Pr_3Sb_3Mg_2O_{14}$, Phys. Rev. B **98**, 134401 (2018).

[44] M. d. Souza, R. Paupitz, A. Seridonio, and R. E. Lagos, Specific heat anomalies in solids described by a multilevel model, Braz. J. Phys. **46**, 206 (2016).